A Self-Resonant Transformer for CLLC Converter

Yam Siwakoti
School of Electrical & Data Engineering
University of Technology Sydney
Sydney, Australia
Yam.Siwakoti@uts.edu.au

Md Imran Hasan
School of Electrical & Data Engineering
University of Technology Sydney
Sydney, Australia
MdImran.Hasan@student.uts.edu.au

Sajib Ahmed
School of Electrical & Data Engineering
University of Technology Sydney
Sydney, Australia
sajib.ahmed@student.uts.edu.au

Aswin Palanisamy
School of Electrical & Data Engineering
University of Technology Sydney
Sydney, Australia
aswin.palanisamy@student.uts.edu.au

Kawsar Ali
Department of Engineering Science
University of Oxford
Oxford, United Kingdom
kawsar.ali@eng.ox.ac.uk

Dan Rogers
Department of Engineering Science
University of Oxford
Oxford, United Kingdom
dan.rogers@eng.ox.ac.uk

Teng Long
Department of Engineering
University of Cambridge
Cambridge, United Kingdom
tl322@cam.ac.uk

***Abstract*—To date, the dominant method of passive component miniaturisation in power converters is through increases in switching frequency, which is enabled by emerging high frequency Wide-Band-Gap devices. However, to push the performance limits for the next generation of high-power-density power converters, research into integrated passive components—such as inductors, capacitors, and transformers into a single structure is essential. This manuscript presents an integrated self-resonating transformer based on Flexible Multilayer Foil (FMLF) for CLLC converters. In this design, all resonant components on both the primary and secondary sides—such as leakage or physical inductance and capacitance—are combined into a single unit, referred to as a Self-Resonant Transformer. This not only reduces the volume, but also the cost and weight of the overall system thereby enabling next-gen highly power dense converters. Moreover, the proposed structure employs a novel trifilar winding configuration to mitigate the effects of bypass capacitance typically observed in conventional winding arrangements. Analysis, design, and experimental measurements are presented to show the efficacy of the proposed structure.**

***Index Terms*—CLLC converter, LLC converter, Passive component integration, Resonant converter.**

I. Introduction

Power converters play a crucial role in modern electronic systems, functioning to convert electrical energy from one voltage level to another efficiently. These converters are central to managing power flow, ensuring stable operation, and maintaining system reliability across diverse applications. However, as the operating frequencies of these converters increase to meet demands for compactness and high-power density, challenges related to efficiency—particularly switching losses—become more pronounced [1]. In response to these challenges, resonant converters have emerged as effective solutions. By employing soft-switching techniques, resonant converters significantly reduce switching losses. However, their reliance on additional passive components (inductors and capacitors) results in increased system size, weight, and cost [2].

In most power converters, the size and layout of the system is largely defined by its passive components and their interconnections. To mitigate this, recent research has explored planar magnetics, integrated magnetics using Flexible Multilayer Foil (FMLF), and passive integration to minimize the quantity, dimensions, and profile of passive components, ultimately improving the power density [3]–[5]. One step further is the integration of passive components, such as L and C for Integrated Power Electronics Module (IPEM) [6], EMI Filter [7] or planer integrated Inductor-Capacitor-Transformer (L-L-C-T) structure, which has been the subject of intensive research over the last few years [8]. This shift towards the integrated passive components is crucial for next-generation applications, including electric vehicles, renewable energy systems, and compact power supplies. A general classification of such passive component integration based on the location of electric and magnetic fields is outlined in Table I. Significant efforts in the literature have focused on integrated magnetics and planar magnetics for unidirectional series resonant converters, such as a LLC.

However, the FMLF-based design offers several advantages over planar structures. It features a shorter winding length, which reduces both copper losses and the overall footprint. Additionally, its layered construction and use of thin dielectric films help minimize eddy current losses and enhance thermal and frequency stability, making it ideal for high-frequency applications [9].

Recent advancements in FMLF technology have enabled

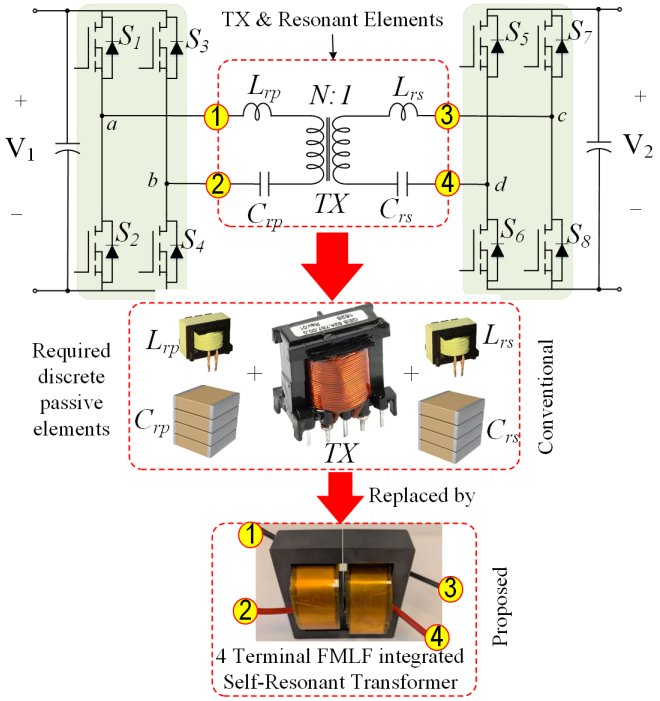

Fig. 1. A concept of 4-terminal Flexible Multilayer Foil (FMLF) Self-Resonant Transformer (SRT) with integrated primary/secondary side L_r and C_r for a series resonant converter.

compact integration of passive components such as inductors, transformers, and capacitors within a single magnetic core. Early works focused on integrated EMI filters, achieving significant volume reduction using interleaved structures, though challenges remained in design complexity, parallel intra-winding capacitance, and reliance on discrete elements [10]. Subsequent efforts extended FMLF integration to micro-inverters, LCL filters for grid-tied applications, and resonant converters, embedding multiple elements within EE cores to improve power density. However, issues such as parallel intra-winding capacitance, limited thermal analysis, and lack of parasitic modelling persisted. To address these gaps, researchers developed analytical and FEM-based models for intra-winding capacitance estimation, facilitating more accurate FMLF structure design. Though these models can estimate the intra-winding capacitance, it is not possible to eliminate this capacitance [11].

In this manuscript, an integrated self-resonating transformer based on FMLF is proposed for series resonant converters with a capability of symmetric bidirectional operation, such as a CLLC. Although an alternative design with decoupled lumped elements is feasible, the proposed approach uses coupled lumped elements to reduce the interconnections (C-L-L-C-T) and enhance the footprint and power density. As a result, the capacitor and inductor terminals are not independently accessible, forming a four-terminal symmetric Self-Resonant Transformer (SRT), as shown in Fig. 1. Moreover, to mitigate the effects of parallel intra-winding capacitance inherent in conventional bifilar winding structures, the proposed design

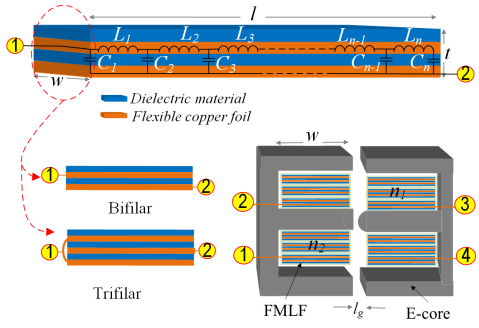

Fig. 2. Cross-section of bifilar/trifilar FMLF and its arrangement in the core (cross sectional view) with an air gap (l_g).

introduces a novel trifilar winding configuration. This new structure effectively reduces the impact of intra-winding capacitance, enhancing the overall performance of the design.

The remainder of the paper is organized as follows: Section II presents the design structure of the proposed self-resonant transformer. Section III details the simulation and experimental results. Finally, Section IV concludes the paper and outlines directions for future work.

II. Proposed Integrated Self-Resonant Transformer

The FMLF is composed of a dielectric layer (blue) and a copper foil (orange), forming a planar capacitor ($C_{1\ldots n}$) that is wrapped around a ferrite core in a coil configuration to enhance the inductance ($L_{1\ldots n}$). A cross section of a simple bifilar/trifilar type FMLF with its transmission line model and its arrangement in the magnetic core is shown in Fig. 2. The core consists of a pair of E-E ferrite cores, where the magnetizing inductance (L_m) and leakage inductance (L_r) of the transformer are determined by properties and dimension of the core and the thickness of air gap (l_g). Here, ($L_{1\ldots n}$) and ($C_{1\ldots n}$) are distributed over the length and not discretely lumped. However, using a first-order approximation, the equivalent circuit of this FMLF achieves the required lumped capacitance (C_{FMLF}) and inductance (L_{FMLF}) required for SRC, as outlined in Table II.

The interaction between the electric ($\vec{E}$) and magnetic ($\vec{B}$) field are minimised to achieve stable characteristics of the inductor, capacitor and transformer over the frequency of interest. In the proposed design, the $\vec{B}$ field generated by the FMLF coil in the ferrite core and the $\vec{E}$ field generated in the FMLF are orthogonal to each other and hence no interaction between the fields is observed. In bifilar FMLF, a significant parallel intra-winding capacitance forms after the winding. This interacts with the series resonant elements and distorts the desired frequency response of the SRT. Hence, trifilar FMLF is selected in the design, which nullifies the parallel intra-winding capacitance whilst doubling the achievable capacitance per unit length in the FMLF. Fig. 3 illustrates the mechanism for nullifying intra-turn capacitance in the proposed trifilar-type FMLF winding structure. A cross-sectional

TABLE I
SUMMARY OF TECHNIQUES USED IN THE LITERATURE TO INTEGRATE INDUCTOR (L), AND CAPACITOR (C).

Method	Illustration of Electric and Magnetic Field	Remarks
Electric field in the winding and magnetic field in the core [3], [4]	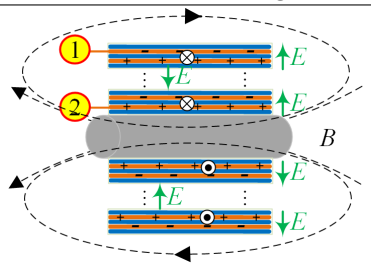	• Electric and magnetic fields do not interact. • Magnetizing current flows through both L and C. • No galvanic isolation between L and C. • Easy design with off-the-shelf components. • Choice of magnetic material does not affect the capacitance and vice versa. • Easy to accommodate air gap. • Off-the-shelf magnetic core: homogeneous distribution of core material.
Electric field and magnetic field co-exist in the core [3], [4]	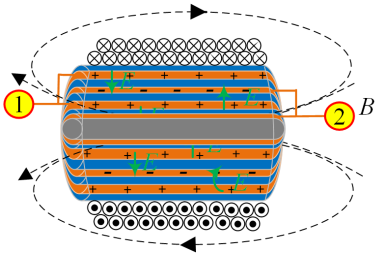	• Electric and magnetic fields interact. • Magnetizing current flows only through L. • Galvanic isolation between L and C. • Need special manufacturing technique. • Choice of magnetic material affect the capacitance and vice versa. • Not so easy to accommodate air gap. • Complex magnetic core: composite of high permeable and dielectric constant core and capacitor electrode.

TABLE II
ILLUSTRATION OF DIFFERENT DESIGN ARRANGEMENT AND THEIR EQUIVALENT LUMPED PARAMETERS.

Design Arrangement	Equivalent Lumped Elements		Inductance	Remarks
	Capacitance Before Winding	Capacitance After Winding		
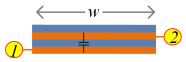 Bifilar	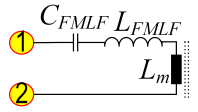 $C_{12} = C_{\text{FMLF}} = \frac{\varepsilon_0 \cdot k \cdot l \cdot w}{t_d}$	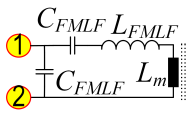 $C_{12} = (C_{\text{FMLF}} \parallel C_{\text{FMLF}}) = 2C_{\text{FMLF}}$	$L_{12} = \frac{\mu_0 \cdot \mu_{\text{eff}} \cdot N^2 \cdot A_e}{l_e}$	The overall thickness of the FMLF is minimal, which reduces the overall footprint of the device. However, a significant parallel intra-winding capacitance forms after the winding. This interacts with the series resonant elements and distorts the desired frequency response of the transformer.
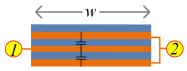 Trifilar	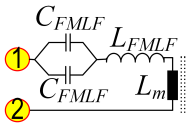 $C_{12} = 2C_{\text{FMLF}}$	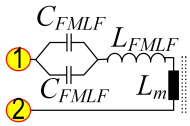 $C_{12} = 2C_{\text{FMLF}}$	$L_{12} = \frac{\mu_0 \cdot \mu_{\text{eff}} \cdot N^2 \cdot A_e}{l_e}$	The overall thickness of the FMLF increases slightly, doubling the required capacitance and nullifying the parallel intra-winding capacitance. Relatively simple to adjust the lumped elements by utilizing the flexibility available in the FMLF dimension.
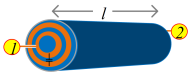 Coaxial	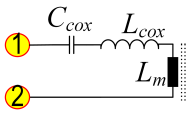 $C_{12} = C_{\text{cox}} = \frac{2\pi\varepsilon_0 kl}{\ln(r_2/r_1)}$	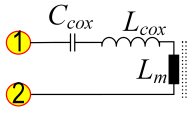 $C_{12} = C_{\text{cox}}$	$L_{12} = \frac{\mu_0 \cdot \mu_{\text{eff}} \cdot N^2 \cdot A_e}{l_e}$	The achievable capacitance per unit length is low. This makes it difficult to tune the required lumped elements at the desired frequency range.

view of a multi-turn FMLF winding around a magnetic core is shown. The structure comprises three conductors: Conductor-1 and Conductor-3 (both shown in blue) are electrically connected at terminals b,d, while Conductor-2 (shown in red) is connected at terminals a,c. Dielectric layers are placed between the conductors to form inter-conductor capacitance, and an additional insulation layer is applied between adjacent turns to ensure electrical isolation. Distributed capacitances are formed between Conductor-1 and Conductor-2, as well as between Conductor-2 and Conductor-3. Intra-turn capacitance

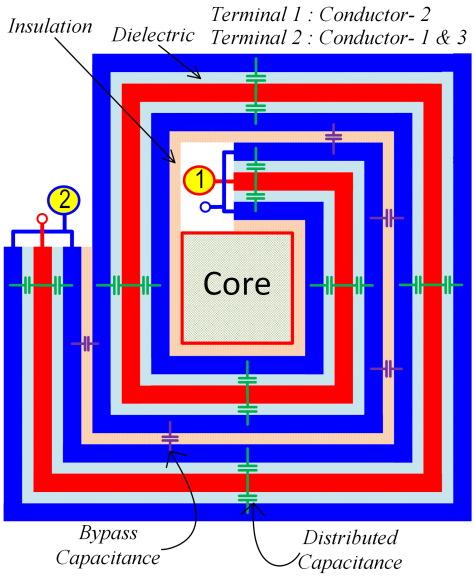

Fig. 3. Cross section of multi-turn winding structure of trifilar type configurations wound around a magnetic core, showing the nullification of intra-turn capacitance.

would typically form between Conductor-1 and Conductor-3; however, since these two conductors are maintained at the same electrical potential, the resulting capacitance is either completely eliminated or reduced to a negligible level. This structural arrangement effectively minimizes intra-turn capacitance within the winding, contributing to improved high-frequency performance.

Additionally, the thickness of the copper foil is carefully selected to be less than the half of skin depth of copper ($t_{cu} \leq 0.5\delta_{cu}$) at the desired frequency of the SRT. Table II summarizes the different possibilities of winding design, their equivalent lumped elements with some remarks. Here, μ_{eff} is the equivalent relative permeability of the magnetic core, A_e is the effective cross sectional area of the core and l_e is the core effective magnetic path length. Only primary side elements/parameters are displayed here due to the nature of symmetry in the design.

III. Simulation and Measurement Results

To verify the above analysis, the developed SRT is first modelled in ANSYS using the parameters as listed in Table III. Polyimide (PI) is used as the dielectric material in this design, with a relative permittivity (dielectric constant) of 3.8 and a dielectric strength of 100 V/μm. Given a dielectric thickness of 0.05 mm (i.e., 50μm), the corresponding breakdown voltage across the dielectric layer is 5kV.

A trifilar FMLF is selected for the SRT design as it eliminates the parallel intra-winding capacitance. The current density, depicted in Fig. 4 with a 5 A excitation (where a bifilar-type FMLF is simulated for clarity), demonstrates that the current is evenly spread across the cross-sectional area of the copper ($w.t_{cu}$). However, along the length of the copper (l), the current varies linearly (either increasing or

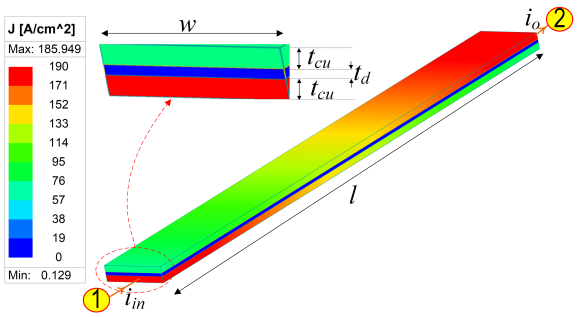

Fig. 4. ANSYS simulation showing the current density in the conductor over the length of the FMLF (scaled down model of bifilar type FMLF with equivalent 5A excitation).

TABLE III
Parameters for Simulations and Prototype.

Parameter/Description	Value/Part Number
Thickness of copper foil (t_{cu})	0.1 mm
Thickness of dielectric (t_d)	0.05 mm
Turns ratio ($n_1 : n_2$)	20:20
Length of the foil (l)	1.5 m
Width of the foil (w)	20 mm
Dielectric constant (K)	3.8
Length of air gap (l_g)	0.5 mm
Magnetic core	E80/38/20-3C94

decreasing), while maintaining $i_{in} = i_o$. A further analysis helps to optimise the conductor thickness for a better form-factor considering skin depth (δ_{cu}) and overall thickness (t) in trifilar or complex FMLF structure.

The magnitude of flux density ($\vec{B}$) distribution considering $\mu - f$ curve of the ferrite core with an air gap of 0.5 mm (Fig. 4) shows that the SRT can safely handle power upto 5 kW@400 Vin without saturation or overheating. Further, various lumped parameters extracted from ANSYS (Fig. 5) shows that their characteristics at the frequency of interest (dc-1MHz) are independent and very stable, ensuring reliable CLLC converter operation.

A four-terminal proof of concept SRT using a trifilar

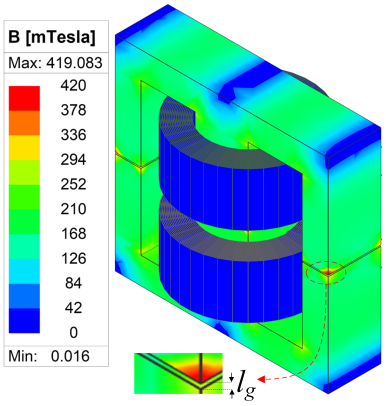

Fig. 5. Magnetic flux density distribution in the SRT core (with 5A excitation).

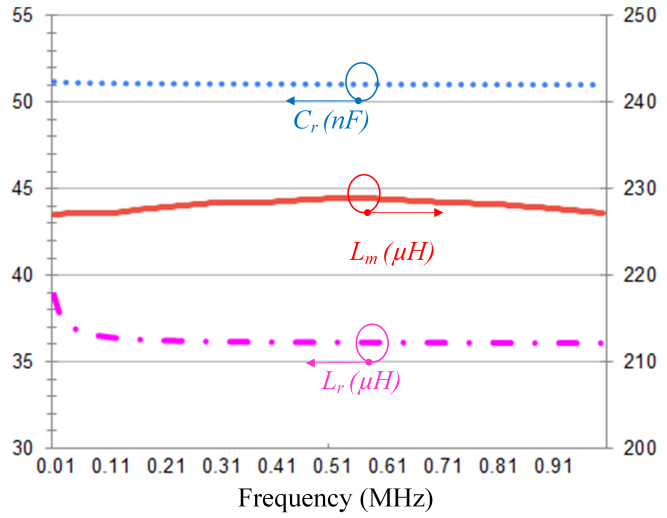

Fig. 6. Frequency characteristics of lumped parameters of SRT over 10 kHz-1 MHz range.

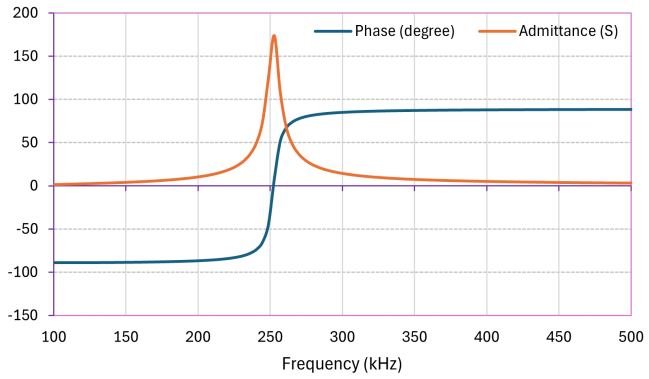

Fig. 7. Measured frequency response of SRT using the PSM1735 Frequency Response Analyzer.

TABLE IV
EXPERIMENTAL PROTOTYPE PARAMETERS.

Parameter	Value
Input Voltage (V_{in})	400.9 V
Input Current (I_{in})	5.71 A
Input Power (P_{in})	2.23 kW
Resistive Load (R)	70.5 Ω
Switching Frequency (f_s)	256.7 kHz

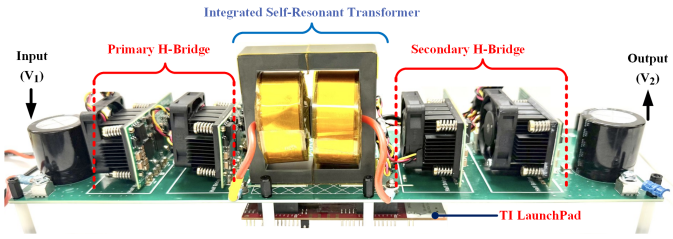

Fig. 8. Test prototype for SRT (CLLC converter).

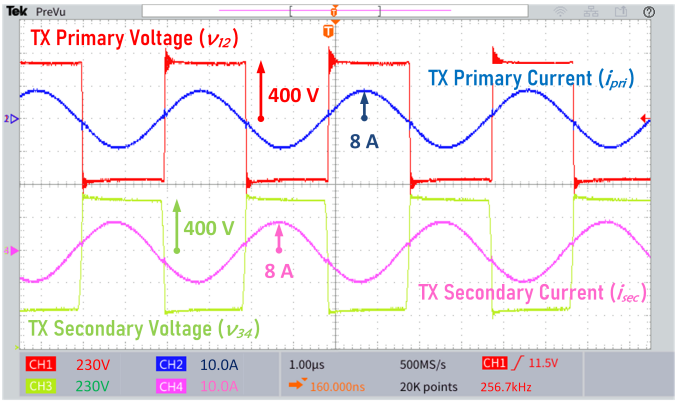

Fig. 9. Measured waveform of SRT with 2.3 kW power, showing primary voltage, primary current, secondary voltage, and secondary current.

FMLF is constructed in the lab using the parameters listed in Table III. Preliminary measurements show a symmetry in parameter measured on either side of SRT. The measured impedance/admittance while the secondary is shorted over 200-300 kHz (Fig. 7) shows a clear first resonant peak at 250 kHz. The SRT is then tested with an active H-Bridge on either side of SRT. Fig. 8 shows the test bench setup used for the experimental demonstration. The measurement was conducted at 2.3 kW, and the parameter ratings are presented in Table IV.

Fig. 9 shows the primary/secondary bridge voltage and primary/secondary current, which are sinusoidal in nature. The resonant frequency of this unoptimized design exceeds the calculated value due to the presence of air pockets between the copper in the FMLF. These air gaps effectively lower the dielectric constant, thereby decreasing the overall capacitance. From Fig. 9 it is observed that at a high input voltage of 400V and an output power of 2.3 kW, the proposed design operates effectively within the CLLC converter without compromizing its soft-switching charecteristics. The magnetic core remained thermally stable and unsaturated, with the temperature not exceeding 40-50°C even after continuous operation for 10-15 minutes at full power. Furthermore, the proposed structure successfully integrates the passive components, thereby reducing overall volume, weight, and cost, while significantly enhancing the power density.

IV. CONCLUSIONS

An integrated SRT based on a FMLF has been developed for a bidirectional CLLC converter. The proposed SRT combines all resonant components from both the primary and secondary sides, minimizing total volume, core loss, and profile, thereby enabling high-power-density CLLC converters. A novel trifilar-type FMLF winding structure has been introduced, aimed at nullifying the intra-turn capacitance formed between adjacent layers. The effectiveness of the proposed SRT has been experimentally validated at 2.3kW power. FEA simulation and experimental results are presented to prove the efficacy of the proposed SRT without sacrificing the perfor-

mance required for the next generation of power converters. Future studies will focus on optimizing the SRT for higher power density and higher power levels (i.e., 5-10 kW), along with a more detailed analysis of current density, skin effect, and proximity effects in the winding structure.

REFERENCES

[1] C. Deng, M. Yong, L. A. G. Rodriguez, J. C. Balda and R. Li, "Passive Integration Using FMLF Technique for Integrated Boost Resonant Converters," in IEEE Transactions on Industrial Electronics, vol. 67, no. 5, pp. 3756-3766, May 2020.

[2] S. Jiang, P. Wang, W. Wang, Y. Liu and D. Xu, "Terminal Configuration Principles for Achieving Various Electromagnetic Integration Units with Flexible Multilayer Foil Technique," in IEEE Electromagnetic Compatibility Magazine, vol. 12, no. 2, pp. 47-61, 2nd Quarter 2023.

[3] A. Schroedermeier and D. C. Ludois, "Integrated Inductor and Capacitor with Co-Located Electric and Magnetic Fields," in IEEE Transactions on Industry Applications, vol. 53, no. 1, pp. 380-390, Jan.-Feb. 2017.

[4] D. C. Ludois and A. L. Schroedermeier, "Integrated capacitor and inductor with low parasitic inductance" U.S. Patent No. 9,934,903.

[5] J. D. van Wyk, et al., "Integrating active, passive and EMI-filter functions in power electronics systems: a case study of some technologies," in IEEE Transactions on Power Electronics, vol. 20, no. 3, pp. 523-536, May 2005.

[6] R. Chen, et al., "Volumetric optimal design of passive integrated power electronics module (IPEM) for distributed power system (DPS) front-end DC/DC converter," in IEEE Transactions on Industry Applications, vol. 41, no. 1, pp. 9-17, Jan.-Feb. 2005.

[7] X. Wu et al., "An integrating structure of EMI filter based on interleaved flexible multi-layer (FML) foils," APEC2009, pp. 491-497.

[8] M. C. Smit, et al, "An ultrasonic series resonant converter with integrated L-C-T" IEEE Trans. Power Electron., vol. 10, no. 1, pp. 25-31, 1995.

[9] C. Deng, S. Li and J. Tang, "A Review of Flexible Multilayer Foil Integration Technology for Passive Components," in IEEE Transactions on Power Electronics, vol. 36, no. 11, pp. 13025-13038, Nov. 2021.

[10] P. Wang, S. Jiang, W. Wei, W. Wang and D. Xu, "Electromagnetic Integration of Decoupled LCL-Filter for Grid-Tied Converters With FMLF Technique," in IEEE Transactions on Power Electronics, vol. 39, no. 1, pp. 649-663, Jan. 2024.

[11] S. Jiang, P. Wang, W. Wang and D. Xu, "Modeling and Design of Full Electromagnetic Integration of a Symmetrical EMI Filtering Circuit With Flexible Multi-Layer Foil Technique," in IEEE Transactions on Electromagnetic Compatibility, vol. 65, no. 2, pp. 414-424, April 2023.